

# Algorithmic Clustering based on String Compression to Extract P300 Structure in EEG Signals\*

Guillermo Sarasa, Ana Granados, Francisco B Rodríguez

## Abstract

*Background and objectives:* P300 is an Event Related Potential control signal widely used in Brain Computer Interfaces. Using the oddball paradigm, a P300 speller allows a human to spell letters through P300 events produced by his/her brain. One of the most common issues in the detection of this event is that its structure may differ between different subjects and over time for a specific subject. The main purpose of this work is to deal with this inherent variability and identify the main structure of P300 using algorithmic clustering based on string compression.

*Methods:* In this work, we make use of the Normalized Compression Distance (NCD) to extract the main structure of the signal regardless of its inherent variability. In order to apply compression distances, we carry out a novel signal-to-ASCII process that transforms and merges different events into suitable objects to be used by a compression algorithm. Once the ASCII objects are created, we use NCD-driven clustering as a tool to analyze if our object creation method suitably represents the information contained in the signals and to explore if compression distances are a valid tool for identifying P300 structure. With the purpose of increasing the level of generalization of our study, we apply two different clustering methods: a hierarchical clustering algorithm based on the minimum quartet tree method and a multidimensional projection method.

*Results:* Our experimental results show reasonable clustering performance over different experiments, showing the structure-extraction capabilities of our procedure. Two datasets with recordings in different scenarios were used to analyze the problem and validate our results, respectively. It has to be pointed out that when the clustering performance over individual electrodes is analyzed, higher P300 activity is found in similar regions to other articles using the same data. This suggests that our approach might be used as an electrode-selection criteria.

*Conclusions:* The proposed NCD-driven clustering methodology can be used to discover the structural characteristics of EEG and thereby, it is suitable as a complementary methodology for the P300 analysis.

---

\*This is the postprint version of an article published in *Computer Methods and Programs in Biomedicine* (Elsevier). The final authenticated version is available online at <https://doi.org/10.1016/j.cmpb.2019.03.009>.

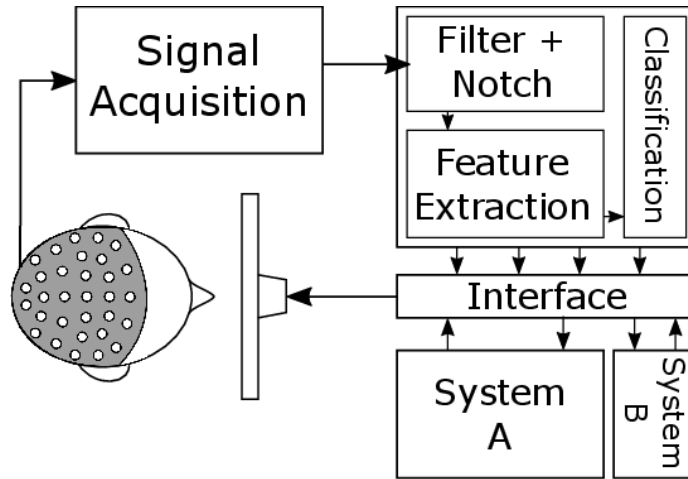


Figure 1: Scheme of a BCI stimuli-based-on system. The signal is recorded by means of certain acquisition technique, for instance the EEG recording. Then the digital signal obtained is processed (filtered + feature extraction + classification) in order to be parsed into commands. Finally, this extracted information (the commands) will be send through an interface with the different systems or devices to do the desired actions (system A and/or system B in figure). These systems can be for instance a commanded wheelchair, a BCI speller to send messages, a commanded robotic arm, etc.

**Keywords:** Normalized Compression Distance; Data Mining; Brain Computer Interface; Similarity; Kolmogorov Complexity; Clustering by Compression; Dendrogram; Multidimensional projections; Silhouette Coefficient;

## 1 Introduction

Brain Computer Interfaces (BCIs) offer a human-computer interaction, translating patterns of brain activity into commands to perform different tasks [1, 2]. BCIs have been used, mostly, by people with motor disabilities, as an external control system, for example, to control a wheelchair or to speak through an artificial voice. The general architecture of a BCI can be seen in Figure 1. First, brain activity is recorded by a (previously defined) signal acquisition technique which contains a pattern as a control signal for the BCI. Next, the signal is filtered and follows several feature extraction methods that aim to improve the BCI precision. Finally, a classifier is trained to discriminate between patterns and communicate, through an interface, with the different systems. Although this architecture can differ between BCI systems, they are usually defined by the acquisition technique and the control signal used.

One of the most commonly used acquisition techniques in the development

of BCIs is Electroencephalogram [3] (EEG). This signal is composed of measurements of brain activity which may contain useful information about the brain state but their non-linear and non-stationary nature makes them very difficult to analyze [4, 5, 6]. Despite this, EEG signals are commonly used in the context of BCI problems due to their time resolution, their low-cost and the fact that they can be easily and non-invasively acquired through electrodes placed on the scalp.

The possibilities and interaction of EEGs are defined by the control signal. Several control signals have been used in the development of BCIs, being the most commonly used in EEG, the so-called Event Related Potentials (ERPs). These are defined as a brain electrophysiological response (very small positive or negative deflections of voltages generated in the brain structures) as a consequence of an external stimulus. Examples of such control signals are the Steady State Visual Evoked Potential [7] (frequency response to visual stimulation), the Sensorimotor Rhythms [3, 8] (subject's will to imagine movements), or the P300 [9, 10] (response to visual, auditory or tactile stimulation). The first two control signals require previous user training while the latter does not. This, in addition to the variety of applications of P300 [11, 12, 13, 14], makes P300s very appealing to be used to develop BCIs. This is the reason why, in this work, we have focused on the P300 control signal.

Typically, a P300 is defined as a positive amplitude increment in the EEG signal due to an infrequent stimulus [9]. Particularly, it is defined as a positive peak in the recorded signal 300 ms after the apparition of a relevant stimulus. P300 is a very complex wave defined by several structural components, some of which have been identified in the literature [15, 14]. Some examples of these structural components are the previous positive deflection potentials, P100 and P200, and the previous negative deflection potentials, N100 and N200 [16, 17]. The latency and amplitude of these components, and many others, may differ making the P300-ERP difficult to identify. Some works have studied this variability [18] and how these factors can vary between subjects (inter-subject variability) [19] and over time for a specific subject (intra-subject variability) [20, 17].

In order to give an insight into how complex and variable the structure of P300 is, six P300 patterns obtained from the same subject are depicted in Figure 2. One can observe that although the six samples correspond to P300 generated by the same person, each of them has particular structures that makes them very different.

On the other hand, there are other issues that may appear in BCI systems: (i) variety between signal sources, (ii) recording of undesired processes or (iii) distortion from the initial acquisition. These reasons, among others, have made that P300s' complex structure had been widely defined and studied.

In this work, we deal with the extraction of P300-ERPs in EEG signals by applying algorithmic clustering based on string compression [21]. In particular, we focus on one of the most successfully applied compression distances: the Normalized Compression Distance (NCD)[22]. This measure has been successfully and widely used due to its parameter-free nature, wide applicability and leading

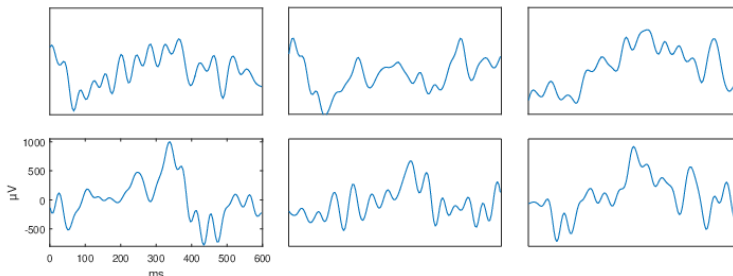


Figure 2: Scheme of six P300-ERPs taken from the II BCI Competition problem 2b (speller matrix) dataset. Each interval, of 600ms, was taken after a stimulus was shown to the subject and the intensified row or column belong to the target character. The P300-ERP should manifest an increment of amplitude around 300ms after the stimulus.

efficacy in numerous domains. Compression distances are powerful tools that allow identification and capture of complex-data structure thanks to the ability that compression algorithms have to analyze data structure in a parameter-free manner. Therefore, we think that compression-based distances could be a useful tool that can help identify P300-ERPs despite their inherent variability. However, in our opinion, the way in which the signal is coded will be crucial for the NCD ability to identify relevant P300 structures. Therefore, we propose a novel signal-to-ASCII process that transforms P300 signals into ASCII objects to help compression algorithms capture P300 structure more accurately. Then, we use clustering as a tool to analyze if our object creation method suitably represents the information contained in the signals and to explore if compression distances are a valid tool for identifying P300. Summarizing, in this work we show how to use clustering based on string compression, in the context of BCI, as a P300 identification methodology.

The rest of the paper is structured as follows. Section 2 presents compression distances and their common application research areas. Section 3 describes the data sets together with the procedures followed to analyze and transform the signal into data objects and the clustering methods performed in our experiments. Section 4 shows our results and some examples of the experiments carried out over the proposed object format and two different datasets, for analysis and validation, respectively. Section 5 presents a briefly review and discussion of our work and the results obtained from the experiments. Finally, Section 6 summarizes the main conclusions of our paper.

## 2 Compression distances

In this work, we propose to use data compression as a tool to distinguish P300 patterns from non-P300 patterns in EEG signals. This can be done thanks to the existence of compression distances, which measure the distance or dissimilarity of two objects using compression algorithms, as described below.

A natural measure of similarity assumes that two objects are similar if the basic blocks of one are part of the other and vice versa. If this happens we can describe one of the objects by making reference to the blocks belonging to the other one. Thus, the description of an object will be very simple using the description of the other one [21]. Compression algorithms can be used to measure the dissimilarity of two objects by applying this idea.

A lossless compressor is a particular case of coding theory in which a mapping is normally defined through a prefix code [23]. This resultant code has a smaller size than the original code. In this way, the compression algorithm works reducing the redundancy in a file by searching for information shared in the whole file. Therefore, a compression algorithm could be used to figure out how redundant two files are if we concatenate them and make the compressor compress the concatenated file. That is, given two files  $x$  and  $y$ , and their concatenated file  $xy$ , if a compression algorithm tried to compress  $xy$ , it would search for information shared by both files ( $x$  and  $y$ ) in order to reduce the redundancy of  $xy$ . If the result were small compared with the compression of each file individually, it would mean that the information contained in  $x$  could be used to code  $y$ .

This was studied by [21, 24], giving rise to the concept of *Normalized Compression Distance* (NCD), whose mathematical formulation is as follows:

$$NCD(x, y) = \frac{\max\{C(xy) - C(x), C(yx) - C(y)\}}{\max\{C(x), C(y)\}},$$

where  $C$  is a compression algorithm,  $C(x)$  is the size of the  $C$ -compressed version of  $x$ ,  $C(xy)$  is the compressed size of the concatenation of  $x$  and  $y$ , and so on. In practice, the NCD is a non-negative number  $0 \leq r \leq 1 + \varepsilon$  representing how different two objects are. Smaller numbers represent more similar objects. The  $\varepsilon$  in the upper bound is due to imperfections in compression techniques, but for most standard compression algorithms, one is unlikely to see an  $\varepsilon$  above 0.1 [21].

The NCD has been applied to numerous research areas because of its parameter-free nature, wide applicability and leading efficacy. For example, among others, it has been applied to data mining [25], profiling diabetes behaviors [26], music clustering [27, 28], document clustering [29, 30], image analysis [31], bird song species classification [32, 33] or video activity recognition [34]. Also, this measure has proved to have a high noise resistance [35] which makes it very appealing for our problem.

To the best of our knowledge, clustering based on string compression has not been applied to the extraction of P300 in EEGs yet. The closest works based

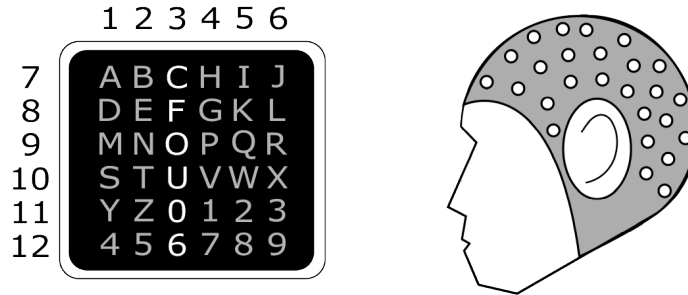


Figure 3: Scheme of a P300 BCI system. The subject pays attention to a speller matrix program in a screen, in which the different columns and rows intensifies randomly. At the same time, the brain activity is recorded through EEG. As a result of row or column intensification of the focused character (marked as \* in figure 4) the signal should increment its amplitude. This increment appears after 300ms and does not last longer that 600ms.

on compression algorithms are [36, 37]. In the former, the authors make use of a quantization technique (Vector Quantization [38] which can be seen as a loss compression mapping), to map the EEG signal into a compressible format. Then, they measure the NCD between the patterns to classify finger movements. The latter makes use of Compressed Sensing, to cast the EEG signals into dictionaries to classify P300-ERPs. There are other works [39, 40, 41, 42, 43] that suggest the use of information-based methodologies to extract information from the signal. In contrast, we reduce the information parsing the signal into ASCII objects and using the NCD, as dissimilarity measure, to identify clusters of similar information among the P300-ERPs.

### 3 Materials and methods

In this section we show the data and methods that have been used to perform the different experiments presented in Section 4. First, we describe the datasets used in our work. Second, we explain how the recorded signals have been split to create two kinds of data objects: objects that contain P300-ERPs and objects without P300-ERPs. Third, we describe the clustering algorithms that have been used in our work. Finally, we explain how the clustering quality has been evaluated.

#### 3.1 Data sets

We have used the data sets of the second BCI Competition [44] (Dataset Iib [45]) and third BCI Competition [46] (Data set II). We have selected these data sets to analyze and study the data through compression algorithms, and to validate our results, respectively. The objective of these competitions is to identify the

characters that a subject spells with a P300 speller [47]. As it is shown in figure 3, a  $6 \times 6$  matrix of characters is presented to a subject. The user is asked to focus attention on a sorted set of characters, one at a time, while different rows and columns are intensified in a random order. For each character to spell, all the rows and columns are intensified, but only 2 of the 12 (6 rows and 6 columns) intensifications should evoke a P300 response in the subject (those that match to the row and the column where the desired character to spell is located). From now on, we will refer to these 12 intensifications as *trial*. This process, or *trial*, is repeated 15 times for each character to spell. That is, for a single character, there would be  $12 \times 15$  intensifications, where 12 corresponds to the number of intensifications required to intensify the 6 rows and the 6 columns of the matrix, and 15 corresponds to the number of repetitions.

In figure 4, we show a sample of the dataset of 2.5 seconds long to show how complex the P300-ERP structure is. In this example, the P300 should manifest as a positive increment of amplitude approximately between 0.5 and 1.0 seconds (following the standard definition of the P300-ERP [9]). Looking closely to this interval, it is possible to glimpse this increment of amplitude. Keep in mind, however, that in some cases the increment of amplitude is not visible at first sight. This is caused by the signal inherit noise and variability.

The dataset of the second BCI Competition (IIb problem) comprises three sessions, but only two of them are labeled. In our work, we only use the labeled ones (called session 10 and session 11 in the dataset). Together both sessions include 42 different characters. As mentioned before, for each character to spell, there will be 180 ( $12 \times 15$ ) intensifications. For each intensification, an interval of 600 ms (144 samples at 240 Hz) is recorded in each channel for a total of 64 electrodes. Hereafter, each of these intervals of 600 ms will be referred to as *segment* (see figure 4). Each of these signal segments is used to create two kinds of objects: those that contain P300 events and those that do not contain this type of event. It is important to notice that, at each session, the characteristics of the recorded data can change for several reasons, being the most important ones: (i) relocation of the electrodes, (ii) differences in the mental state of the subject, and (iii) adaptation of the subject as new experiments are performed. For these reasons, we performed different experiments for each session, both separately and jointly.

Besides, in order to increase the level of generalization of our results, we have used another dataset, particularly the third BCI Competition, Dataset II. The objective of this competition is also to identify characters spelled by a subject with a P300 speller. However, in this case, two subjects were asked to spell a total of 85 characters instead of 42. A very interesting point is that the quality of the recorded EEG signal is fairly worse than the quality of the signal from the second BCI Competition (IIb problem). This fact is given by the score obtained by the winners of both competitions. While in the second competition there is a tie (5 people) in the first position with a 1.0 [48] classification rate, in the third competition the maximum score is below 0.96 [49], followed by a 0.9 [50]. Using the third BCI competition dataset allows us to validate the capabilities of our method with a signal of worse quality. Thus, we expect to find a decrease

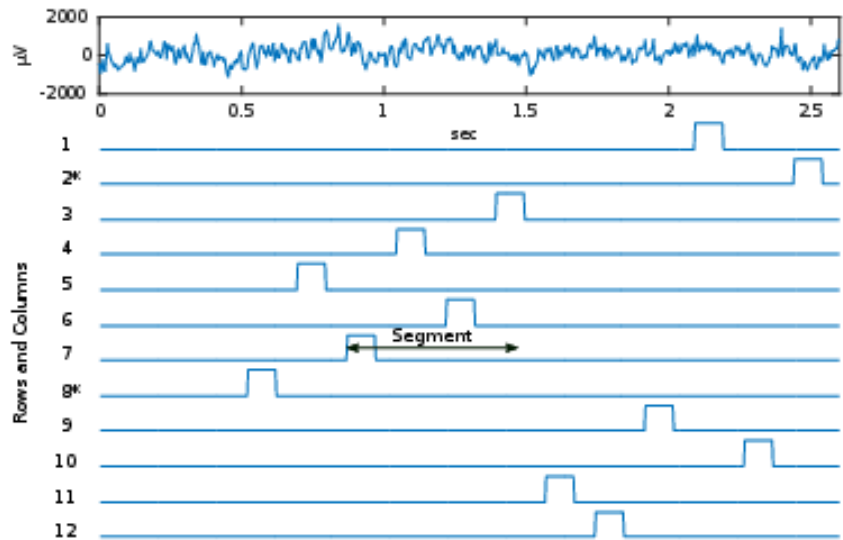


Figure 4: Structure used in the recording session showed in figure 3. This figure is a reduced but more detailed version of figure 2. Each numbered source correspond to each stimulus (rows 1-6, and columns 7-12) of the speller matrix, where each pulse corresponds to an intensification of that row or column. Once the infrequent stimulus appears, an amplitude increment should appear in the recorded signal 300 ms. The change generated by the ERP should not continue 600ms after the stimulus. After the marked row and column should manifest a P300-ERP in the figure. In this case, the subject was paying attention to the character “E” according to figure 3.

in the clustering quality in contrast with the BCI Competition II.

### 3.2 Signal processing: Object definition

Our experience working with the NCD in different research areas [34, 33, 30, 51] tells us that the way in which the signal is coded is crucial for the NCD ability to identify relevant P300 structures [29, 52]. Therefore, we process the EEG signal parsing it into objects through the following process: First, the signal is band passed between 0.5 and 10 Hz (following [49], through a Butterworth filter) and standardized to minimize the undesired components. Then, the segments from filtered and standardized data are extracted and stored in vectors to be later labeled as P300 or non-P300, depending on whether the stimulus corresponds to the intensification of the target row/column or not. As mentioned above, for every stimulus showed to the subject, a 600ms interval is stored (see figure 4). Please note that since there are a total of 6 rows and 6 columns, there will be five times more objects in the non-P300 class than in the P300 class.

Once all the labeled vectors have been stored, each object is created by com-



binning three operations: random selection of segments, average of the selected segments and concatenation of several averages, as figure 5 shows. First, several segments from one class are randomly chosen (see figure 5 (A)). Second, the selected segments are averaged (see figure 5 (B)). Third, several products of the averaging process are combined to create one object (see figure 5 (C)). Accordingly, the object creation can be parameterized with two parameters: number of selected segments to average ( $M$ ) and number of selected concatenations ( $C$ ).

It is important to point out that the reason for applying an average process is to improve the capabilities of extracting P300 features by reducing the inherent noise of the signal. It has to be highlighted that this averaging approach has been widely used in other BCI solutions. On the other hand, the concatenation process aims to improve the accuracy of compression distances. The idea behind the concatenation process is to build the object with several examples of averages. In this way, the object is more general because of the different examples that it contains of the class that it represents.

Owing to the parametrization of the objects which includes the number of segments used to calculate the averaged segments ( $M$ ), and the number of averaged segments concatenated ( $C$ ), the objects may differ in each experiment. Thus, as it will be described in Section 4, we have explored the effect that changing these parameters has on the quality of the obtained results.

### 3.3 From the NCD to data clusters

In this work we explore if the NCD can be used to distinguish between P300-ERPs and non-P300-ERPs, which depends on whether compression distances are able to capture P300 structure or not. For this purpose, we first create ASCII objects from EEG signals, as explained in Section 3.2. Then, a NCD matrix that contains all the pairwise distances between every pair of objects is calculated. This matrix can be seen as a reduced form of the information representing the original dataset, however, in this format, this information cannot be easily analyzed. That is the reason why we use clustering to transform the information contained in the NCD matrix to a cognitively acceptable format. In other words, we transform a NCD matrix into data clusters. We proceed like this because the most usual ways to measure NCD matrix grouping capabilities is through clustering techniques such as hierarchical clustering and multidimensional mapping [21, 53].

Therefore, in this work, we use clustering as a tool to analyze if our object creation method suitably represents the information contained in the signals and to explore if compression distances are a valid tool for identifying P300. In this manner, we use the NCD matrix as input to a clustering method and we analyze the performance of the clustering by analyzing the quality of the clusters provided by the clustering method. In an ideal clustering all P300 objects would be clustered together, and the same would happen to all non-P300 objects. Summarizing, if our ASCII objects suitably represented the information contained in EEG signals and the NCD were a valid tool for identifying P300, we would obtain high quality clustering results.

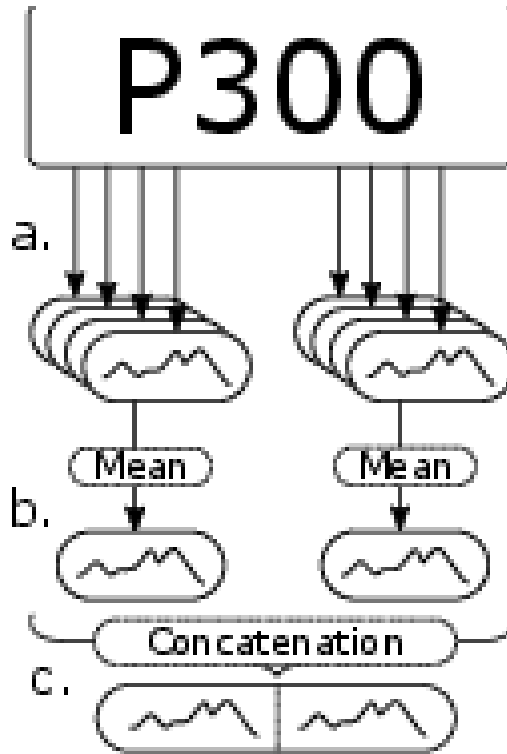


Figure 5: Scheme followed in the object definition. For each intensification of the two target stimuli (row-column of the target character that should contain a P300-ERP), our system creates a first object (A) (which will be stored in a common set). Then, all these objects were shuffled and grouped together in subsets of  $M$  elements in order to average each one of them, and compose the second objects (B). Finally, the group process is repeated to concatenate each subset in groups of  $C$  objects into the final objects (C). In this figure  $M = 4$  and  $C = 2$ . This process is repeated for the non-P300 objects as well.

With the purpose generalizing our results, we apply two different clustering methods. First, we use the one presented in [21], developed by the creators of the NCD. This is a hierarchical clustering algorithm based on the minimum quartet tree method that takes a NCD matrix as input and generates a dendrogram as output [54, 21]. Second, we use another clustering method that can work with NCD matrices. This is a multidimensional mapping algorithm based on multidimensional projections (Nearest Neighbors Projection) [55, 56] that takes a NCD matrix as input and generates a projection as output. It is important to point out that multidimensional projections use a different approach from hierarchical clustering methods based on dendrogram representation. Using two clustering methods of such different nature allows us to increase the level

of generalization of our study. The following sections describes both clustering algorithms in depth.

### 3.3.1 Minimum quartet tree method (CompLearn)

The first approach used in our work consists of using an algorithm based on the minimum quartet tree method. In terms of implementation, we use the CompLearn Toolkit [54], which implements the clustering algorithm described in [21]. This algorithm has an asymptotic cost of  $\mathcal{O}(N^3)$  (CompLearn version 1.1.5). Therefore, there is a limitation in the size of the data sets, due to the convergence costs of this algorithm. Once the NCD matrix is calculated, it is used as input to the clustering phase and a dendrogram is generated as output.

A dendrogram is an undirected binary tree diagram, frequently used for hierarchical clustering, that illustrates the arrangement of the clusters produced by a clustering algorithm. In figure 6, we can observe an example of dendrogram obtained from the BCI Competition II data set [44], using an object configuration of  $C = M = 4$  (a combination of four concatenations and four averages of ERP segments for each object). That is, each object is created by averaging 4 segments to obtain the “averaged segments” and concatenating 4 “averaged segments” afterwards. In our work, the “quality” of any dendrogram obtained as output from this process, has been measured using an adaptation of the Silhouette coefficient (taking the path between leaves as their distance), as explained in Section 3.4.

### 3.3.2 Multidimensional projections (PEX)

The second approach consists of visualizing high-dimensional data through mapping techniques taking the NCD matrix as input to build a multidimensional projection. Several ways of visualizing high-dimensional data through mapping techniques exist in the literature. In general terms, a mapping technique gives each datapoint a location in a two or three dimensional map [57]. This allows a human to visually analyze datasets because they are represented in a two or three dimensional map. In terms of implementation, we use the Projection Explorer (PEX), a visualization tool that takes a distance matrix as input and generates a projection through mapping techniques [57, 58].

This approach allows us not only to corroborate that the NCD can be used to detect P300 in EEG but also to represent more samples in a visually resilient way. As mentioned above, PEX, in contrast to CompLearn, has fewer limitations about the number of objects used in the analysis. In figure 7, we show an output example of PEX over a subset of objects previously built as described in Section 3.2. The configuration of the objects is  $C = M = 4$ , and like in figure 6, it represents an preliminary result of our work. In this case the Silhouette Coefficient is measured by the PEX software using the Euclidean distance between each pair of objects.

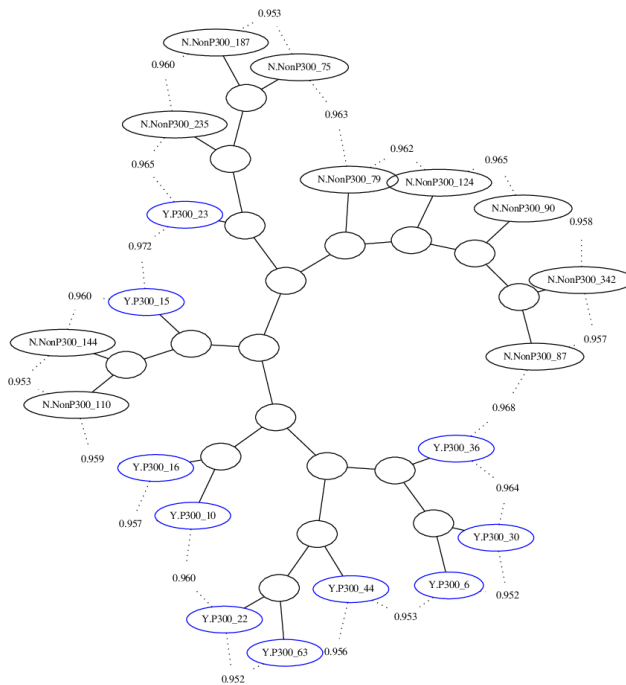


Figure 6: Sample of a CompLearn’s hierarchical tree [54] from a subset of objects, of the second BCI Competition. CompLearn is a compression based toolbox that takes, in this case, the NCD distance matrix as input and generates a hierarchical tree. The configuration used was  $C = M = 4$ , according to the method described in figure 5. The blue nodes correspond to the P300s objects and the black ones to the non-P300. The Silhouette Coefficient of the dendrogram is 0.3474.

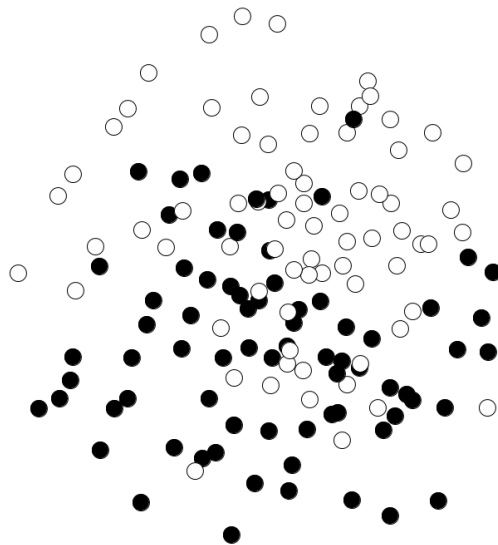


Figure 7: Sample of a PEX's projection from a subset of objects, of the second BCI Competition. PEX is a visualization tool that takes, in this case, the NCD distance matrix as input and generates a projection through mapping techniques. [56, 53]. Following the method described in figure 5, we take the same object configuration of figure 6, where  $M = C = 4$ . The white nodes correspond to the P300s objects and the black ones to the non-P300s. The Silhouette Coefficient of the projection is 0.1352

### 3.4 Data cluster quality in the Dendrogram: Silhouette Coefficient

The main objective of this work is to explore whether a compression-based clustering methodology could extract a single P300-ERP structure regardless of the variability contained in the EEG signal. Then, using the described methods in the previous section, this can only happen if the output of the clustering shows a single cluster for the P300 group. Thereby, we make use of the Silhouette Coefficient (SC) [59] to measure the cohesiveness of each cluster compared to the other cluster. Thus, the coefficient which defines the relation of an object with the clusters is defined as follows:

$$s(i) = \frac{b(i) - a(i)}{\max\{a(i), b(i)\}}, \quad (1)$$

where the measure  $a(i)$  is the average distance of  $i$  with all other objects within the same cluster, and  $b(i)$  is the average lowest distance of  $i$  to the nearest other cluster. Finally, the Silhouette coefficient of the whole dataset is calculated averaging  $s(i)$  over all objects of the entire dataset.

Hence, the score given by the SC will be reinforced by low values of  $a(i)$  and high values of  $b(i)$ . In other words, by similar objects within the cluster and dissimilar clusters within the set. The PEx toolkit [53] uses the average Euclidean distance between nodes (objects in this case) to calculate  $a(i)$  and  $b(i)$ .

However, in order to measure the SC from a dendrogram we have adapted its general definition to our specific domain, following [29]. Thus, with the aim of calculating the SC in a dendrogram, we define the distance,  $d\{i, j\}$ , between each pair of objects (or dendrogram leaves), as the number of nodes between  $i$  and  $j$ . Thus, the distances  $a(i)$  and  $b(i)$  have been defined as follows for this specific case:

$$a(i) = \frac{1}{n} \sum_{j \in C_i} d\{i, j\}, \quad b(i) = \frac{1}{m} \sum_{j \notin C_i} d\{i, j\},$$

where  $n$  is the number of elements of its cluster ( $C_i$ ) and  $m$  is the number of elements of the cluster more similar to object  $i$  and different from  $C_i$ .

## 4 Experimental results

In this section, we show the experiments that have been carried out. First, we explore how changes in the number of segments used to assemble the objects affect the identification of P300 in the EEG signal. For this analysis a single electrode as data source is used. Second, we study the activity of P300 events in all the 64 electrodes used in standard BCI schemes. Third, we combine the information of several electrodes to study the optimal objects' configuration.

That is, we perform a detailed study on the effects of changing the parameters  $M$  and  $C$  when several electrodes are used. Finally, we carry out some experiments over a different dataset to generalize our results.

#### 4.1 Preliminary study: means and concatenations

The purpose of this preliminary study is to gain intuition about how much information can be identified in the objects depending on the parameter configuration used to create them. That is, depending on the values of  $M$  (means) and  $C$  (concatenations) used to create the objects as described in Section 3.2. In order to do this, we have briefly studied the impact that changing the parameters  $M$  and  $C$  has on the clustering quality. In this regard, two different experiments have been carried out.

The objects for both experiments have been generated using a single electrode as data source. More particularly, we have taken a reference data source for the detection of the P300, the so-called Cz electrode position according to [60]. We have chosen this electrode because it is well known that it reports good results in the classification of P300-ERPs [4, 61].

After creating the objects, we have calculated the NCD for every pair of nodes. Then, using this matrix as input, we have clustered the objects by means of two different methods: CompLearn and PEx, obtaining dendrograms and projections, respectively, as output to the methods. Finally, the clustering quality has been quantified using the Silhouette Coefficient (SC).

For the first experiment, and due to the limited number of P300-ERPs in the dataset, we limited the number of segments per object to 64 to maintain a minimum number of objects per projection. Thus, we have created objects using four different configurations: (i)  $M = C = 1$ , (ii)  $M = 1, C = 8$ , (iii)  $M = 8, C = 1$ , (iv)  $M = C = 8$ . By visual inspection of figure 8, it can be observed that incrementing the number of segments used to create the objects, seems to improve the separation of P300 and non-P300 objects. In this case, the configuration which gives us the best projection is the one with  $M = C = 8$ . This phenomenon is also slightly visible in the raw distances between P300 and non-P300 objects.

Looking at table 1, one can notice that the average NCD between the two groups is higher as the number of ERPs per object grows. Particularly, in the first case ( $C = M = 1$ ) the difference is  $\sim 10^{-5}$  while in the second case ( $C = M = 8$ ) is  $\sim 10^{-3}$ . This means that the objects are 100 times different (on average) in the second case compared with the first one. Which means that the resolution of the NCD will be better and thereby, the final clustering.

In order to dig into this preliminary result, we have created more sets of objects using more configurations, with  $M = C$ , and we have studied how the clustering quality depends on the number of segments used to create the objects. We have explored only configurations where  $M = C$  because the purpose of this preliminary study is not to analyze the impact of  $M$  and  $C$  separately, but to corroborate that incrementing the number of segments used to create the objects improves the quality of the clustering results (figure 9). It can be observed that

<b>C = M = 1</b>	<b>P300s</b>	<b>non-P300s</b>	<b>diff</b>
	0.98612	0.98617	$\sim 10^{-5}$
<b>C = M = 1</b>	<b>P300s</b>	<b>non-P300s</b>	<b>diff</b>
	0.95246	0.95592	$\sim 10^{-3}$

Table 1: Average NCD between the different pairs of groups of objects for two different configurations. The upper table shows the different values measured in a sample of objects assembled with  $C = M = 1$  configurations. In this case one can observe a small difference between the average inner-group distance and inter-group distance ( $\sim 10^{-5}$ ). On the other hand, using a higher configuration ( $C = M = 8$ ), depicted in the lower table, the differences between these two measures are bigger ( $\sim 10^{-3}$ ). Thus, looking at the average difference distance between groups (forth column), we can see an improvement of 100 times in the second case compared with the first one. An example of these two  $C$  and  $M$  configurations is depicted in figure 8.

the clustering quality improves as the number of segments increases, as the first experiment suggested. However, it is necessary to carry out a broad study on the effects of changing the parameters  $M$  and  $C$  separately using more electrodes to derive more conclusions (see Section 4.3).

We have to point out that for the analysis presented in this section, we have used the well-known Cz electrode because the P300-ERP is measured very strongly in this electrode. A logical question that arises is: what happens with other electrodes where P300-ERP is not measured so strongly. The goal of next section is to analyze this question by extending the previous analysis to all the 64 electrodes to observe if the differences in the strength of P300-ERP measurement are congruent with the quality of the clustering obtained.

## 4.2 Scoring sources

The purpose of this experiment is studying the activity of the P300 in all the electrodes. The experiment that has been carried out is similar to the last experiment presented in previous section. That is, the parameters  $M$  and  $C$  are equal, particularly,  $M = C = 8$ .

For each electrode, we have limited the number of objects per dendrogram to 20. In this case, the number of objects have been chosen to overcome the convergence limitations of CompLearn. Thus, as a consequence of this, we have repeated the process 100 times. In order to summarize the results of each electrode, we have measured the SC of each dendrogram and depicted each distribution both as a boxplot and a scalp colormap. This allows an easy comparison of the electrodes depending on their position on the scalp.

Figure 10 depicts the SC obtained for all the 64 electrodes, using the data of both sessions (see Section 3.1). Looking at both the boxplot and scalp distributions, a couple of observations can be made. First, due to the SC distribution, we notice that the structure of the P300-ERP is not manifested equally among



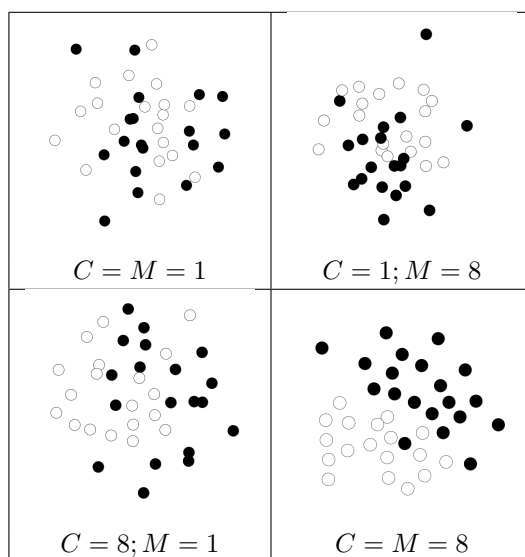


Figure 8: Output of PEx from different object configurations, for a single electrode (Cz according to [60]). We observed in this experiment that the increment of segments per object seems to improve the separation of both clusters. In order to compare each configuration we take a subset of objects for each one of them due to the last configuration, Lower-right, that can not generate more than 18 P300 objects.

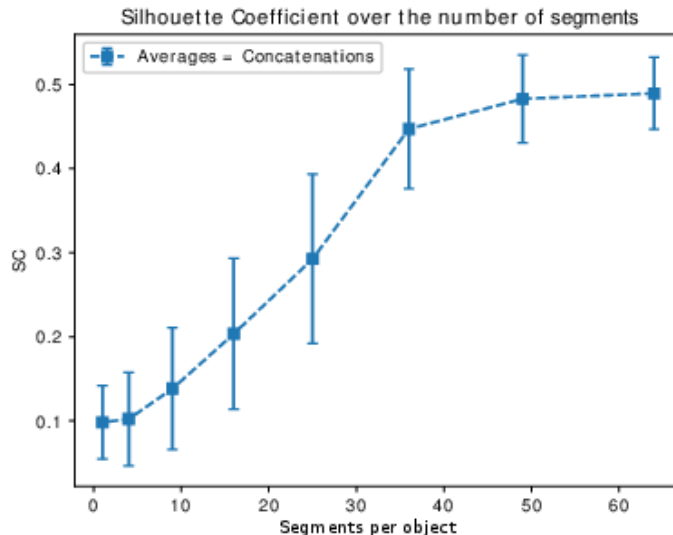


Figure 9: Simulation over the number of segments per object (single P300-ERPs or non-P300-ERPs) for an unique electrode (Cz according to [60]) through Maketree’s clustering. Each data point represents the average of iterating 100 times the simulation (20 files per simulation due to cost limitations of Maketree algorithm). The data was taken from both training sessions (10 and 11). The iterated parameters were the number of segments used in both concatenation and average processes. In this case, the curve only represents those configurations with equal number of segments for both concatenation and average processes (i.e.  $M = C$ ).

the electrodes, as it is well known [15, 62, 4]. Second, we observed that there are three main areas (corresponding to the warm colors in the scalp) where the structure of the P300-ERP appears more clearly. These areas are similar to the ones obtained in other works of P300-EEG context [62, 63]. This fact, supports the idea of a good ERP structure identification by our methodology. This phenomenon also appears in the individual analysis for sessions 10 and 11.

Analyzing each session alone, as it is shown in figures 11 and 12, one can observe that the objects created from the data corresponding to session 10 provide better clustering results than the data from session 11 according to [64]. This difference between sessions may be caused by several reasons. Among many others, there may be a relocation of the electrodes or some changes in the mental state of the subject. In this case, giving these results, we believe that, in general, the session 11 may contain a worse signal quality than the first one.

Summarizing, in this section we have explored how the P300 signal is distributed along all electrodes for a fixed configuration of objects ( $M = C = 8$ ). Hence, for the single-electrode analysis, we have observed that the P300-ERP is

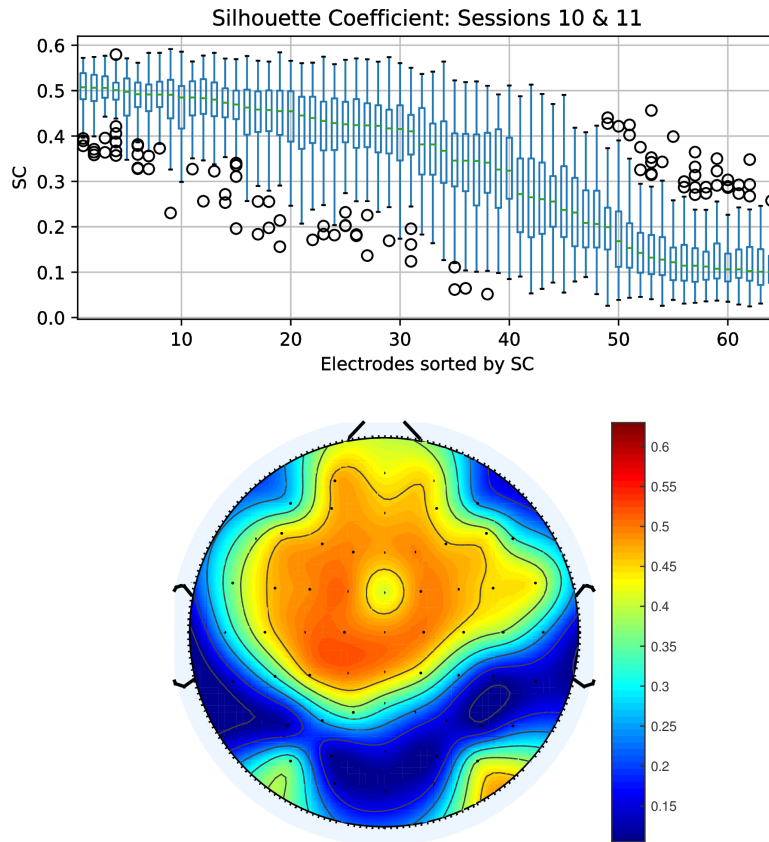


Figure 10: Silhouette Coefficient distribution obtained for each electrode for both sessions 10 and 11. Each score was calculated from a  $M = C = 8$  configuration from 100 iterations of CompLearn simulation. The upper figure shows the SC distribution among electrode through boxplots. The lower figure shows the median of the SC for each electrode across the scalp.

not equally distributed among the electrodes, as it is well know. This fact can be seen in figures 10, 11 and 12. Also, we have located some areas where the ERP activity is clearer, which agree with previous results reported in the literature [62, 63]. In the next section we will study which combination of concatenations and means, in the creation of objects, improves the separation between P300 and non-P300.

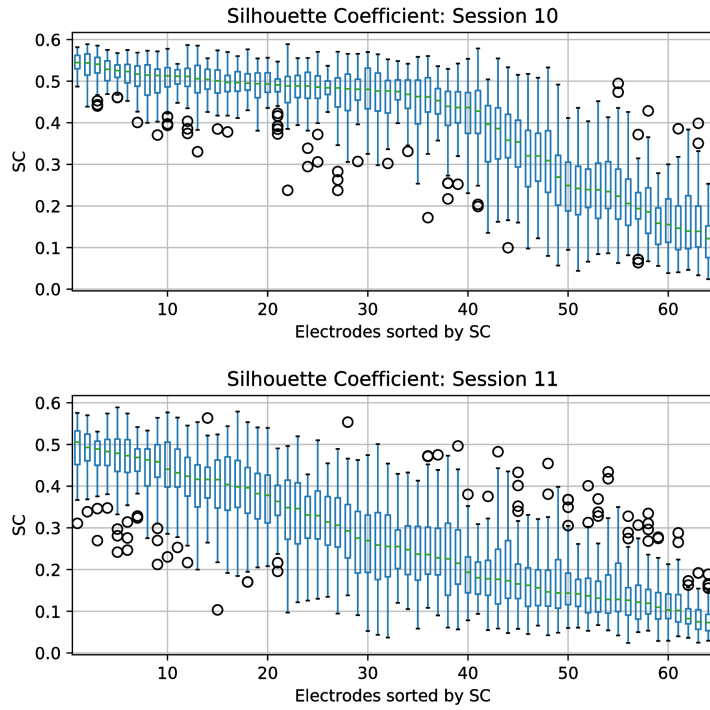


Figure 11: Silhouette Coefficient boxplot distribution obtained for each electrode for sessions 10 and 11, individually. Each score was calculated from a  $C = M = 8$  configuration from 100 iterations of CompLearn simulation.

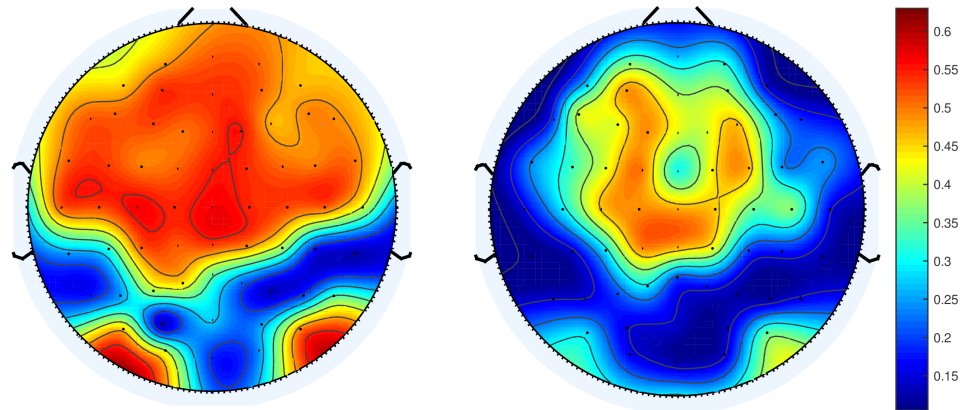


Figure 12: Silhouette Coefficient means distribution across the scalp obtained for each electrode for sessions 10 (left) and 11 (right), individually. Each score was calculated from a  $C = M = 8$  configuration from 100 iterations of CompLearn simulation.

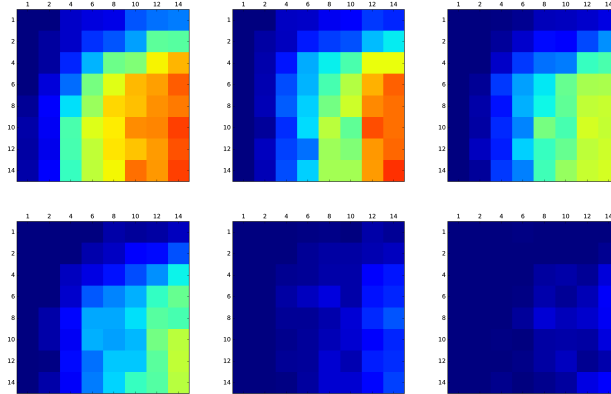
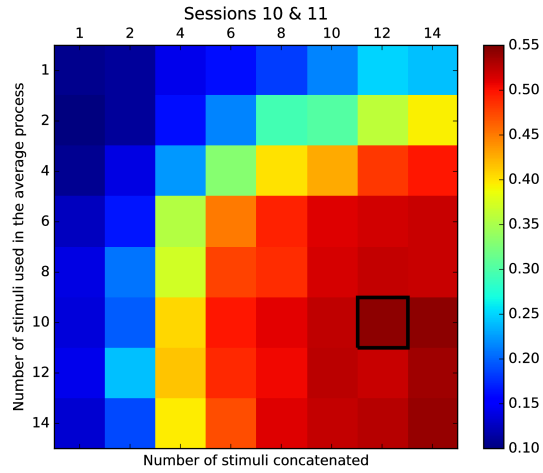


Figure 13: Grid simulation over the number of ERPs used in both the average and concatenation processes. In the first color map, the first 8 electrodes with higher SC were used to perform the simulation. These 8 electrodes, also, correspond to the center-frontal area of the scalp. The other 6 color maps show the results for the following 6 subsets of 8 electrodes, from higher SC to lower. The black square shows the best configuration obtained in the entire simulation.

Configuration	Subsets of Electrodes						
	0 - 7	8 - 15	16 - 23	24 - 31	32 - 39	40 - 47	48 - 55
C1 M1	0.1121	0.1044	0.0879	0.0847	0.0972	0.0898	0.0978
C4 M4	0.2371	0.1944	0.1702	0.1355	0.1367	0.1116	0.1108
<b>C12 M4</b>	<b>0.4209</b>	0.3093	<b>0.2070</b>	0.1917	0.1723	0.1053	0.1021
<b>C4 M12</b>	<b>0.4818</b>	0.4048	<b>0.3813</b>	0.3296	0.2445	0.1626	0.1290
C12 M12	0.5294	0.4564	0.4362	0.3858	0.3616	0.1607	0.1235

Table 2: Silhouette Coefficients from some configurations of Means (M) and Concatenations (C) from figure 13, for different sets of electrodes. The columns represent the different subsets of electrodes used in each experiment (e.g. 0-7 represents the first 8 electrodes sorted by activity, and so on). The rows of the table represent the different object configurations used in each experiment. Looking at the configurations C4 M12 and C12 M4, one can notice difference in the clustering quality obtained from each configuration even though the number of ERPs used is the same. Also, the “degradation” in the SC caused by taking worse sets of electrodes, tends to affect less the configurations with higher Concatenations than those with higher Means. This phenomenon is particularly more visible between the first and third configurations (highlighted in bold). In the first case the SC difference between the two configurations is  $\sim 0.006$  while in the second one is  $\sim 0.1743$ .

### 4.3 Grid Search in Object Comparison

As presented in Section 4.1, we have observed that the clustering quality seems to be correlated with the number of segments used to create each object. However, we have explored limited configurations of the parameters  $M$  and  $C$ . With the aim of analyzing the impact that both parameters have on the clustering quality, we have performed a more exhaustive grid search.

In this experiment, we have explored configurations from  $M = 1$  to  $M = 14$  and from  $C = 1$  to  $C = 14$ . Besides, instead of using single electrodes, we have used 8 electrodes in each experiment. Each subset of electrodes has been selected based on the SC obtained in the experiments presented in Section 4.2. Hence, we have sorted the electrodes according to their median SC, and we have created several sets of electrodes (the first set contains the best 8 electrodes, the second set contains the electrodes in positions 9 to 16, and so on). Figure 13 depicts the obtained results for the first 7 subset of electrodes to show the obtained progression. Some interesting numerical values of SC that correspond to Figure 13 are presented in Table 2, to show a more detailed version of this experiment.

As we expected, analyzing figure 13 and Table 2, it can be noticed that the combination of the best electrodes provides greater SC than the combination of those electrodes with lower SC. We have also observed some differences between the parameters  $M$  and  $C$ , that is, between the average and concatenation processes. Thus, while the concatenation process always increases the SC, the average process increases it until  $M = 6$ . In the table 2, one can see that

while the configuration of  $M = 4$  and  $C = 12$  reports a SC of 0.48, for the best subset of electrodes, the opposite configuration ( $M = 12; C = 4$ ) reports a SC of 0.42, even though they use the same number of ERPs per object (48). The fact that the number of ERPs used in the concatenation process seems to be more important than the ones used in the averaged process can be observed looking at the other configurations of the table.

Our hypothesis is that the average reduces the noise of the segments but does not provide enough information to generalize the method which, in this case, is provided by the concatenation. On the other hand, neither the average nor the concatenation processes alone can identify the structure of the objects well enough, probably due to the combination of noise and differences between P300-ERPs.

Finally, we have repeated the experiments performed for figures 6 and 7 when the combination of means and concatenations was not optimized. In these new experiments we have taken the best combination of  $C$  and  $M$ , following the previous experiments of figure 13 ( $M = 10$  and  $C = 12$ ). As we show in figures 14 and 15, the separation between both clusters is improved compared to the previous experiments. It is interesting to point out, however, that the SC obtained for both methods, PEx and CompLearn, differs in magnitude. This is caused by the differences in the measurement of the SC (described in section 3.4).

#### 4.4 Validation and generalization of results to extract P300-ERPs

Along this paper, we have performed different experiments to analyze and study the capabilities of a clustering analysis based on string compression to identify P300-ERP structure. Now, in this section, we aim to validate our previous results using a different dataset: BCI Competition III, dataset II [46]. Particularly, we have performed the same experiments of Sections 4.2, to obtain the best electrodes of each subject, and 4.3, to achieve a reasonable P300-ERP clustering, to this dataset.

First, following a methodology similar to the one followed in the experiment of figure 10, we have obtained the electrode SC map for both subjects A and B (see figure 16). The configuration used in this case is the same as in the previously mentioned experiment,  $C = M = 8$ . In these figures, one can observe that the areas of activity are more isolated in the third competition than in the experiments of the second competition. This is given by the signal quality differences between both competitions. Also, these results (the activity regions) are consistent with the ones showed by the winners of the competition in [49], which may suggest that our method is capable of extracting relevant information for a P300-ERP analysis.

Using the data gathered for the previous experiment (depicted in figure 17), we have combined the best electrodes of the central-frontal zone (as in figure 13) into a unique dendrogram, in order to improve the overall clustering. For both subjects, we have used the same configuration used in the experiment of

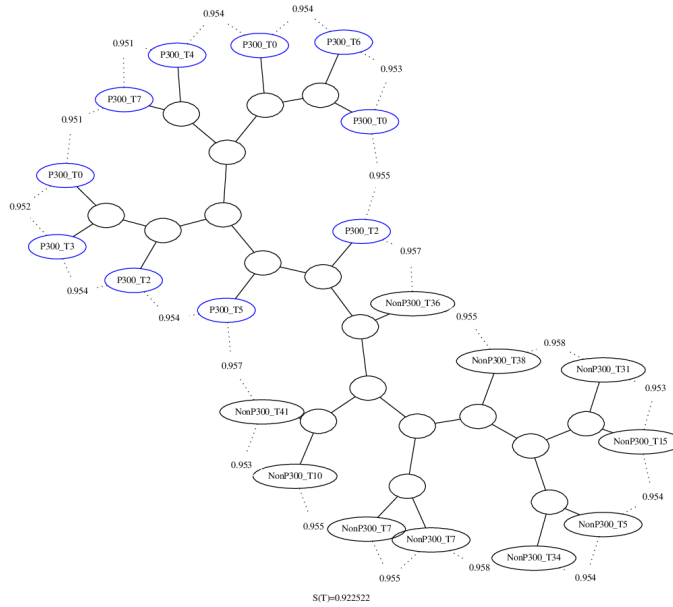


Figure 14: Dendrogram (using CompLearn toolkit) obtained from a subset of optimized objects. The blue nodes correspond to P300s objects and the black ones to non-P300. The Silhouette Coefficient of the dendrogram is 0.56. Following the scheme of figure 5, we take a configuration for objects creation of  $M = 10$  and  $C = 12$ . This configuration corresponds to the optimal separation of P300 and non-P300 in figure 13. Here, we can see how the separation of P300 and non-P300 from figure 6, where the number of means and concatenations was not optimized, is improved considerably.



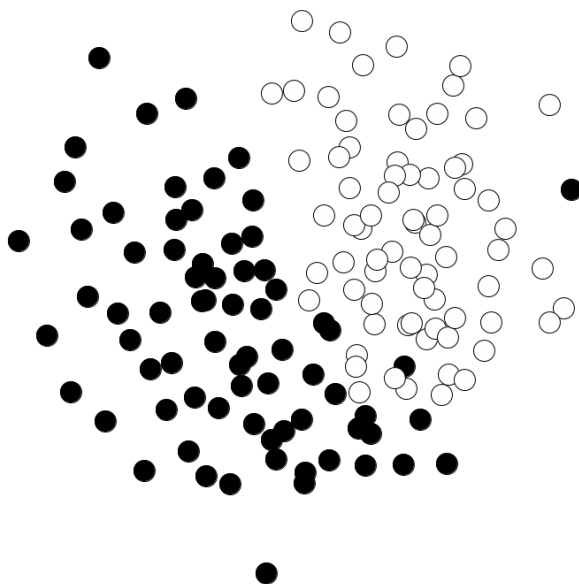


Figure 15: PEx projection from a subset of optimized objects. The white nodes correspond to the P300 objects and the black ones to non-P300. The Silhouette Coefficient of the projection is 0.36. Following the scheme of figure 5, we take a configuration of  $M = 10$  and  $C = 12$ . This configuration corresponds to the optimal separation of P300 and non-P300 in figure 13. Here, we can see how the separation of P300 and non-P300 from figure 7, where the number of means and concatenations was not optimized, is improved considerably.

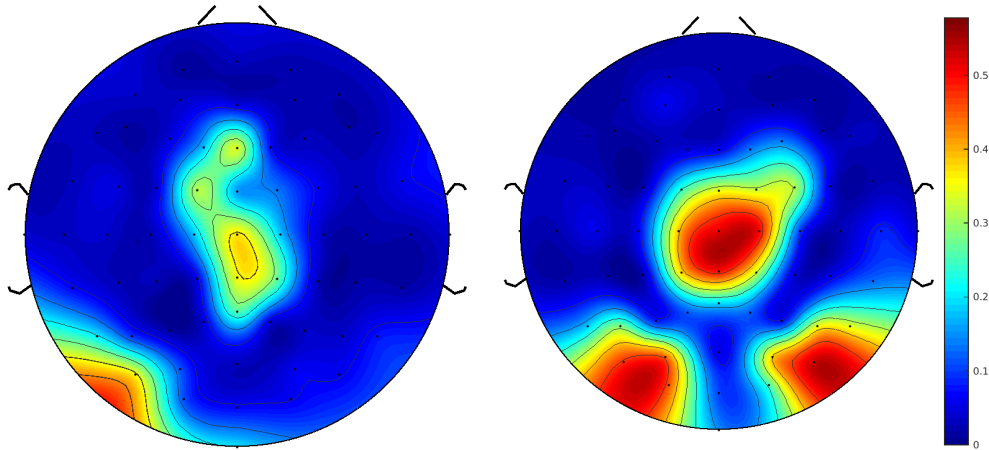


Figure 16: Silhouette Coefficient means distribution across the scalp obtained for each electrode for the subject A and B, respectively, of the third BCI Competition. Each score was calculated from a  $C = M = 8$  configuration with CompLearn.

figure 15, ( $C = 12$  and  $M = 10$ ). In this experiment, we have observed that combining electrodes of the same zone with a high SC improves the clustering, as we observed using the same method over the data set of the second BCI Competition. On the other hand, we have observed that the number of electrodes with high clustering quality is fairly lower in the BCI Competition III data set, which make sense given the signal quality differences between both competitions.

## 5 Discussion

Throughout this work, we have carried out several experiments to test the capabilities of our NCD-driven clustering methodology. Firstly, we have explored how varying the parameters of our object-creation method affects the clustering performance, preliminary in Section 4.1 and more detailed in Section 4.3. For our experiments, we have taken two different clustering methods to double-check our results, and the Silhouette Coefficient as an unbiased quality measure. The results obtained from these experiments have showed a tendency for better clustering with higher numbers of P300-ERPs per file. In figures 8 and 9 this fact is slightly visible, but it is clear in Figure 13. In the experiments of the last figure, we noticed slight differences alternating between averages and concatenations per file, being the concatenation of P300-ERPs apparently more important than their average in the long term. In our opinion, the average of a few P300-ERPs may be sufficient for removing the majority of noise and variability from an object. On the other hand, the concatenation of several P300-ERPs in one ob-

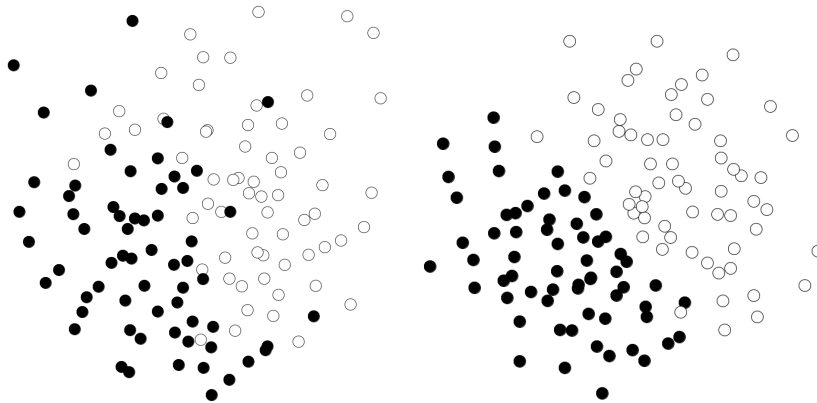


Figure 17: PEx projection from Subject A and B, respectively, obtained from the top 3 central-frontal subset of optimized objects from the BCI Competition III dataset II. The white nodes correspond to the P300 objects and the black ones to non-P300. The Silhouette Coefficient of the projections are 0.25 and 0.38, respectively. The configuration is  $M = 10; C = 12$ .

ject, which can be seen as multiple examples, can provide more generalization to the final objects. Besides, the concatenation process increases the size of objects, which in scenarios where dealing with small objects, always improves the capabilities of the NCD [21, 65].

Finally, the last experiments presented in the paper were targeted to produce a score for each electrode. These experiments were carried out to compare our approach with other works in the literature. Congruent results were obtained first in Section 4.2 as a proof of concept, and second in Section 4.4 using a different dataset to validate our previous results. In these experiments, we have found remarkable differences between the activity of the two datasets used in this paper, which is also congruent with the classification scores published in the website of each dataset. Thus, while in the first competition five different contestant achieved 0% error in the classification, only one contestant achieved an error below 4% in the second one (followed by a 9.5 % error).

## 6 Conclusions

The first objective of this work was to explore whether compression-based distances could be a useful tool for identifying P300 structure. Derived from this, the second objective of this work was to develop a method to represent ERP-based EEG signals in a manner that compressors are able to identify common structures between different P300-ERPs. Therefore, we have defined a signal-to-ASCII process to parse the EEG signal into objects so that they are suitable to be used by a compression algorithm. The results obtained show that the NCD can be successfully applied to the P300 identification using our coding

methodology. We have found consistent results in the P300 activity regions with other works in the literature. This fact not only validates our method of object representation, but confirms that compression-based distances are a valid tool for analyzing P300.

## Acknowledgement

This work was funded by Spanish project of Ministerio de Economía y Competitividad/FEDER TIN2014-54580-R and TIN2017-84452-R ( <http://www.mineco.gob.es/> ). The funder had no role in study design, data collection and analysis, decision to publish, or preparation of the manuscript. We thank Diana Flores for helping us with the SC measurement of the dendrogram.

## References

- [1] R. P. N. Rao, *Brain-Computer Interfacing: An Introduction*, Cambridge University Press, 2013.
- [2] S. Amiri, R. Fazel-Rezai, V. Asadpour, S. Amiri, R. Fazel-Rezai, V. Asadpour, A Review of Hybrid Brain-Computer Interface Systems, A Review of Hybrid Brain-Computer Interface Systems, *Advances in Human-Computer Interaction*, *Advances in Human-Computer Interaction* 2013, 2013 (2013) e187024.
- [3] S. Arroyo, R. P. Lesser, B. Gordon, S. Uematsu, D. Jackson, R. Webber, Functional significance of the mu rhythm of human cortex: an electrophysiologic study with subdural electrodes, *Electroencephalography and Clinical Neurophysiology* 87 (3) (1993) 76–87.
- [4] D. J. Krusienski, M. Grosse-Wentrup, F. Galán, D. Coyle, K. J. Miller, Elliott Forney, C. W. Anderson, Critical issues in state-of-the-art brain–computer interface signal processing, *Journal of Neural Engineering* 8 (2) (2011) 025002.
- [5] L. F. Nicolas-Alonso, J. Gomez-Gil, *Brain Computer Interfaces, a Review*, *Sensors (Basel, Switzerland)* 12 (2) (2012) 1211–1279.
- [6] D. McFarland, J. Wolpaw, Eeg-based brain–computer interfaces, *Current Opinion in Biomedical Engineering* 4 (2017) 194 – 200, *synthetic Biology and Biomedical Engineering / Neural Engineering*.
- [7] S. T. Morgan, J. C. Hansen, S. A. Hillyard, Selective attention to stimulus location modulates the steady-state visual evoked potential., *Proceedings of the National Academy of Sciences of the United States of America* 93 (10) (1996) 4770–4774.

- [8] H. Yuan, B. He, Brain-computer interfaces using sensorimotor rhythms: current state and future perspectives, *IEEE transactions on bio-medical engineering* 61 (5) (2014) 1425–1435.
- [9] T. W. Picton, The P300 wave of the human event-related potential, *Journal of Clinical Neurophysiology: Official Publication of the American Electroencephalographic Society* 9 (4) (1992) 456–479.
- [10] S. Gao, Y. Wang, X. Gao, B. Hong, Visual and Auditory Brain-Computer Interfaces, *Ieee Transactions on Biomedical Engineering* 61 (5) (2014) 1436–1447.
- [11] T. Kaufmann, A. Herweg, A. Kübler, Toward brain-computer interface based wheelchair control utilizing tactually-evoked event-related potentials, *Journal of NeuroEngineering and Rehabilitation* 11 (2014) 7.
- [12] S. Halder, I. Kaethner, A. Kuebler, Training leads to increased auditory brain-computer interface performance of end-users with motor impairments, *Clinical Neurophysiology* 127 (2) (2016) 1288–1296.
- [13] T. Fukami, J. Watanabe, F. Ishikawa, Robust estimation of event-related potentials via particle filter, *Computer Methods and Programs in Biomedicine* 125 (2016) 26–36.
- [14] Y. Chen, Y. Ke, G. Meng, J. Jiang, H. Qi, X. Jiao, M. Xu, P. Zhou, F. He, D. Ming, Enhancing performance of P300-Speller under mental workload by incorporating dual-task data during classifier training, *Computer Methods and Programs in Biomedicine* 152 (2017) 35–43.
- [15] B. Blankertz, S. Lemm, M. Treder, S. Haufe, K.-R. Müller, Single-trial analysis and classification of ERP components—a tutorial, *NeuroImage* 56 (2) (2011) 814–825.
- [16] G. A. Light, N. R. Swerdlowa, M. L. Thomas, M. E. Calkins, M. F. Green, T. A. Greenwood, R. E. Gur, R. C. Gur, L. C. Lazzeroni, K. H. Nuechterlein, M. Pela, A. D. Radant, L. J. Seidman, R. F. Sharp, L. J. Siever, J. M. Silverman, J. Sprock, W. S. Stone, C. A. Sugar, D. W. Tsuang, M. T. Tsuang, D. L. Braff, B. I. Turetsky, Validation of mismatch negativity and P3a for use in multi-site studies of schizophrenia: Characterization of demographic, clinical, cognitive, and functional correlates in COGS-2, *Schizophrenia Research* 163 (1-3) (2015) 63–72.
- [17] G. Ouyang, A. Hildebrandt, W. Sommer, C. Zhou, Exploiting the intra-subject latency variability from single-trial event-related potentials in the P3 time range: A review and comparative evaluation of methods, *Neuroscience & Biobehavioral Reviews* 75 (2017) 1–21.
- [18] M. Fira, L. Goras, Comparison of Inter-and Intra-Subject Variability of P300 Spelling Dictionary in EEG Compressed Sensing, *International*

Journal of Advanced Computer Science and Applications 7 (10) (2016) 366–371.

- [19] R. van Dinteren, M. Arns, M. L. A. Jongsma, R. P. C. Kessels, P300 Development across the Lifespan: A Systematic Review and Meta-Analysis, PLoS ONE 9 (2) (2014) e87347.
- [20] J. Lu, W. Speier, X. Hu, N. Pouratian, The effects of stimulus timing features on P300 speller performance, Clinical Neurophysiology 124 (2) (2013) 306–314.
- [21] R. Cilibrasi, P. M. B. Vitanyi, Clustering by compression, IEEE Transactions on Information Theory 51 (4) (2005) 1523–1545.
- [22] M. Li, X. Chen, X. Li, B. Ma, P. M. B. Vitanyi, The similarity metric, IEEE Transactions on Information Theory 50 (12) (2004) 3250–3264.
- [23] D. Salomon, M. G., Handbook of Data Compression, Springer London, 2010.
- [24] M. Li, X. Chen, X. Li, B. Ma, P. Vitanyi, The Similarity Metric, IEEE Transactions on Information Theory 50 (12) (2004) 3250–3264.
- [25] R. Cilibrasi, P. M. Vitanyi, The Google Similarity Distance, IEEE Transactions on Knowledge and Data Engineering 19 (3) (2007) 370–383.
- [26] I. Contreras, C. Quirós, M. Giménez, I. Conget, J. Vehi, Profiling inpatient type I diabetes behaviors, Computer Methods and Programs in Biomedicine 136 (2016) 131–141.
- [27] A. González-Pardo, A. Granados, D. Camacho, F. de Borja Rodríguez, Influence of Music Representation on Compression-based Clustering, in: IEEE World Congress on Evolutionary Computation, 2010, pp. 2988 – 2995.
- [28] D. Meredith, Compression-based geometric pattern discovery in music, in: 2014 4th International Workshop on Cognitive Information Processing (CIP), 2014, pp. 1–6.
- [29] A. Granados, K. Koroutchev, F. d. B. Rodríguez, Discovering Data Set Nature through Algorithmic Clustering Based on String Compression, IEEE Transactions on Knowledge and Data Engineering 27 (3) (2015) 699–711.
- [30] A. Granados, M. Cebrian, D. Camacho, F. d. B. Rodríguez, Reducing the Loss of Information through Annealing Text Distortion, IEEE Transactions on Knowledge and Data Engineering 23 (7) (2011) 1090–1102.

- [31] A. Cohen, C. Bjornsson, S. Temple, G. Banker, B. Roysam, Automatic Summarization of Changes in Biological Image Sequences Using Algorithmic Information Theory, *IEEE Transactions on Pattern Analysis and Machine Intelligence* 31 (8) (2009) 1386–1403.
- [32] G. Sarasa, A. Granados, F. B. Rodriguez, An approach of algorithmic clustering based on string compression to identify bird songs species in xeno-canto database, in: 2017 3rd International Conference on Frontiers of Signal Processing (ICFSP), 2017, pp. 101–104.
- [33] G. Sarasa, A. Granados, F. B. Rodriguez, Automatic Treatment of Bird Audios by Means of String Compression Applied to Sound Clustering in Xeno-Canto Database, in: V. Kůrková, Y. Manolopoulos, B. Hammer, L. Iliadis, I. Maglogiannis (Eds.), *Artificial Neural Networks and Machine Learning – ICANN 2018, Lecture Notes in Computer Science*, Springer International Publishing, 2018, pp. 617–625.
- [34] G. Sarasa, A. Montero, A. Granados, F. B. Rodriguez, Compression-Based Clustering of Video Human Activity Using an ASCII Encoding, in: V. Kůrková, Y. Manolopoulos, B. Hammer, L. Iliadis, I. Maglogiannis (Eds.), *Artificial Neural Networks and Machine Learning – ICANN 2018, Lecture Notes in Computer Science*, Springer International Publishing, 2018, pp. 66–75.
- [35] M. Cebrian, M. Alfonseca, A. Ortega, The Normalized Compression Distance is Resistant to Noise, *IEEE Transactions on Information Theory* 53 (5) (2007) 1895–1900.
- [36] P. Berek, M. Prilepok, J. Platos, V. Snasel, Classification of EEG Signals Using Vector Quantization, in: L. Rutkowski, M. Korytkowski, R. Scherer, R. Tadeusiewicz, L. A. Zadeh, J. M. Zurada (Eds.), *Artificial Intelligence and Soft Computing*, no. 8468 in *Lecture Notes in Computer Science*, Springer International Publishing, 2014, pp. 107–118.
- [37] M. Fira, L. Goras, On the Size of the Universal Dictionaries Used in EEG P300 Spelling Paradigm Based on Compressed Sensing, in: *Proceedings of the 9th International Conference on Bioinformatics and Biomedical Technology, ICBBT '17*, ACM, New York, NY, USA, 2017, pp. 28–32.
- [38] Vector Quantization and Signal Compression | Allen Gersho | Springer.
- [39] C. Alagoz, A. R. Cohen, D. R. Frisch, B. Tuğ, S. Phatharodom, A. Guez, Spiral waves characterization: Implications for an automated cardiodynamic tissue characterization, *Computer Methods and Programs in Biomedicine* 161 (2018) 15–24.
- [40] N. Kannathal, M. L. Choo, U. R. Acharya, P. K. Sadasivan, Entropies for detection of epilepsy in EEG, *Computer Methods and Programs in Biomedicine* 80 (3) (2005) 187–194.

- [41] E. Bonmati, A. Bardera, I. Boada, Brain parcellation based on information theory, *Computer Methods and Programs in Biomedicine* 151 (2017) 203–212.
- [42] R. Baravalle, O. A. Rosso, F. Montani, Discriminating imagined and non-imagined tasks in the motor cortex area: Entropy-complexity plane with a wavelet decomposition, *Physica A: Statistical Mechanics and its Applications* 511 (2018) 27–39.
- [43] J. Gibson, Entropy Power, Autoregressive Models, and Mutual Information, *Entropy* 20 (10) (2018) 750.
- [44] BCI Competition II, <http://www.bbcii.de/competition/ii/>.
- [45] 2nd Wadsworth BCI Dataset.  
URL [http://www.bbcii.de/competition/ii/albany\\_desc/albany\\_desc\\_ii.html](http://www.bbcii.de/competition/ii/albany_desc/albany_desc_ii.html)
- [46] BCI Competition III, <http://www.bbcii.de/competition/iii/>.
- [47] C. S. Nam, A. Nijholt, F. Lotte, *Brain-Computer Interfaces Handbook: Technological and Theoretical Advance*, CRC Press, 2018.  
URL <https://hal.inria.fr/hal-01655819>
- [48] B. Blankertz, K. R. Muller, G. Curio, T. M. Vaughan, G. Schalk, J. R. Wolpaw, A. Schlogl, C. Neuper, G. Pfurtscheller, T. Hinterberger, M. Schroder, N. Birbaumer, The BCI competition 2003: progress and perspectives in detection and discrimination of EEG single trials, *IEEE Transactions on Biomedical Engineering* 51 (6) (2004) 1044–1051.
- [49] A. Rakotomamonjy, V. Guigue, BCI Competition III: Dataset II- Ensemble of SVMs for BCI P300 Speller, *IEEE Transactions on Biomedical Engineering* 55 (3) (2008) 1147–1154.
- [50] B. Blankertz, K. R. Muller, D. J. Krusienski, G. Schalk, J. R. Wolpaw, A. Schlogl, G. Pfurtscheller, J. R. Millan, M. Schroder, N. Birbaumer, The BCI competition III: validating alternative approaches to actual BCI problems, *IEEE Transactions on Neural Systems and Rehabilitation Engineering* 14 (2) (2006) 153–159.
- [51] A. González-Pardo, A. Granados, D. Camacho, F. d. B. Rodríguez, Influence of music representation on compression-based clustering, in: *IEEE Congress on Evolutionary Computation*, 2010, pp. 1–8.
- [52] A. Granados, D. Camacho, F. B. Rodríguez, Is the contextual information relevant in text clustering by compression?, *Expert Systems with Applications* 39 (10) (2012) 8537–8546.



- [53] F. V. Paulovich, M. C. F. Oliveira, R. Minghim, The Projection Explorer: A Flexible Tool for Projection-based Multidimensional Visualization, in: XX Brazilian Symposium on Computer Graphics and Image Processing, 2007. SIBGRAPI 2007, 2007, pp. 27–36.
- [54] R. Cilibrasi, A. L. Cruz, S. de Rooij, M. Keijzer, CompLearn Home, CompLearn Toolkit, [Online] Available: <http://www.complearn.org/>.
- [55] C. Feng, B. Yang, Projection search for approximate nearest neighbor, in: 2016 17th IEEE/ACIS International Conference on Software Engineering, Artificial Intelligence, Networking and Parallel/Distributed Computing (SNPD), 2016, pp. 33–38.
- [56] G. P. Telles, R. Minghim, F. V. Paulovich, Normalized compression distance for visual analysis of document collections, *Computers & Graphics* 31 (3) (2007) 327–337.
- [57] F. V. Paulovich, M. C. F. Oliveira, R. Minghim, The projection explorer: A flexible tool for projection-based multidimensional visualization, in: Proceedings of the XX Brazilian Symposium on Computer Graphics and Image Processing, SIBGRAPI '07, 2007, pp. 27–36.
- [58] G. Telles, R. Minghim, F. Paulovich, Normalized Compression Distance for Visual Analysis of Document Collections, *Computers & Graphics* 31 (3) (2007) 327–337.
- [59] P. J. Rousseeuw, Silhouettes: A graphical aid to the interpretation and validation of cluster analysis, *Journal of Computational and Applied Mathematics* 20 (1987) 53–65.
- [60] T. D. Lagerlund, F. W. Sharbrough, C. R. Jack, B. J. Erickson, D. C. Strelow, K. M. Cicora, N. E. Busacker, Determination of 10-20 system electrode locations using magnetic resonance image scanning with markers, *Electroencephalography and Clinical Neurophysiology* 86 (1) (1993) 7–14.
- [61] D. D. Didoné, M. V. Garcia, S. J. Oppitz, T. F. F. da Silva, S. N. dos Santos, R. S. Bruno, V. A. V. d. S. Filha, P. L. Cóser, Auditory evoked potential P300 in adults: reference values, *Einstein* 14 (2) (2016) 208–212.
- [62] M. T. McCann, D. E. Thompson, Z. H. Syed, J. E. Huggins, Electrode subset selection methods for an EEG-based P300 brain-computer interface, *Disability and Rehabilitation. Assistive Technology* 10 (3) (2015) 216–220.
- [63] L. Li, C. Gratton, M. Fabiani, R. T. Knight, Age-related frontoparietal changes during the control of bottom-up and top-down attention: an ERP study, *Neurobiology of Aging* 34 (2) (2013) 477–488.
- [64] N. Xu, X. Gao, B. Hong, X. Miao, S. Gao, F. Yang, BCI competition 2003-data set IIb: enhancing P300 wave detection using ICA-based subspace projections for BCI applications, *IEEE Transactions on Biomedical Engineering* 51 (6) (2004) 1067–1072.

- [65] A. Granados, R. Martínez, D. Camacho, F. d. B. Rodríguez, Improving NCD accuracy by combining document segmentation and document distortion, *Knowledge and Information Systems* 41 (1) (2014) 223–245.